Alzheimer's & Dementia 11 (2015) 964-974

Florbetaben PET imaging to detect amyloid beta plaques in Alzheimer's disease: Phase 3 study

Osama Sabri[a,*,1], Marwan N. Sabbagh[b,1], John Seibyl[c], Henryk Barthel[a], Hiroyasu Akatsu[d,e,f], Yasuomi Ouchi[g], Kohei Senda[h], Shigeo Murayama[i,j], Kenji Ishii[j], Masaki Takao[j,k], Thomas G. Beach[b], Christopher C. Rowe[l], James B. Leverenz[m,3], Bernardino Ghetti[n], James W. Ironside[o], Ana M. Catafau[p], Andrew W. Stephens[p], Andre Mueller[p], Norman Koglin[p], Anja Hoffmann[q], Katrin Roth[q], Cornelia Reininger[q,1], Walter J. Schulz-Schaeffer[r,1], and for the Florbetaben Phase 3 Study Group[2]

[a]*Department of Nuclear Medicine, University of Leipzig, Leipzig, Germany*
[b]*Banner Sun Health Research Institute, Sun City, AZ, USA*
[c]*Molecular Neuroimaging LLC, New Haven, CT, USA*
[d]*Fukushimura Hospital, Toyohashi, Japan*
[e]*Department of Community-based Medicine, Nagoya City University Graduate School of Medical Sciences, Nagoya City, Aichi, Japan*
[f]*Department of Neurology, Nagoya City University Graduate School of Medical Sciences, Nagoya City, Aichi, Japan*
[g]*Department of Biofunctional Imaging, Medical Photonics Research Center, Hamamatsu University School of Medicine, Hamamatsu, Japan*
[h]*Koseikai Hospital, Toyohashi, Japan*
[i]*Department of Neurology and Neuropathology, Tokyo Metropolitan Geriatric Hospital & Institute of Gerontology, Tokyo, Japan*
[j]*Tokyo Metropolitan Institute of Gerontology, Tokyo, Japan*
[k]*Mihara Memorial Hospital, Isesaki, Japan*
[l]*Department of Molecular Imaging, Austin Health, University of Melbourne, Melbourne, VIC, Australia*
[m]*VA-Puget Sound Health Care System and University of Washington, Seattle, WA, USA*
[n]*Department of Pathology and Laboratory Medicine, Indiana University School of Medicine, Indianapolis, IN, USA*
[o]*Centre for Clinical Brain Sciences, University of Edinburgh, Edinburgh, Scotland*
[p]*Piramal Imaging GmbH, Berlin, Germany*
[q]*Bayer Pharma AG, Berlin, Germany*
[r]*Department of Neuropathology, University Medical Center Göttingen, Göttingen, Germany*

Conflict of interest disclosures: Osama Sabri received research grants, consultant and speaker honoraria and travel expenses from Bayer Healthcare/Piramal Imaging. Marwan W. Sabbagh has contracts or grants with Bayer Healthcare, Piramal Imaging, Navidea Biopharmaceuticals, Avid, GE Healthcare, Avanir, Elan, Functional Neuromodulation, Eisai, Pfizer, and Genentech, is a consultant for Lilly, Avid, Piramal Imaging, Biogen and Eisai, and receives royalties from Ten Speed and Wiley. John Seibyl holds equity interest in Molecular Neuroimaging and is a consultant to Piramal Imaging and GE Healthcare. Henryk Barthel received research grants, consultant and speaker honoraria and travel expenses from Bayer Healthcare/Piramal Imaging. Work by Hiroyasu Akatsu was partially supported by funding from Bayer. Kenji Ishii has been a paid consultant to GE Healthcare. Thomas G. Beach is a consultant for Avid Radiopharmaceuticals, GE Healthcare and Navidea Biopharmaceuticals, and has a research contract with Navidea Biopharmaceuticals. Christopher C. Rowe has received research grants from Bayer Schering Pharma. James B. Leverenz is a consultant with Bayer, Citibank, Piramal Imaging, and Navidea Biopharmaceuticals. James W. Ironside was a consultant with Covance UK, Bayer and Piramal Imaging and has received honoraria from Springer and Elsevier. Bernardino Ghetti was a consultant with Bayer and Piramal Imaging and has a research contract with Eli Lilly. Ana M. Catafau, Andrew W. Stephens, Andre Mueller, and Norman Koglin are employees of Piramal Imaging GmbH, Berlin, Germany. Anja Hoffmann and Katrin Roth are employees of Bayer Pharma AG, Berlin, Germany. Cornelia Reininger was an employee of Bayer Healthcare and is now an employee of Navidea Biopharmaceuticals as Chief Medical Officer. Walter J. Schulz-Schaeffer received research grants from Bayer Healthcare and Piramal Imaging. The other authors declare no competing interests.

[1]Contributed equally.[2]Listed in the Acknowledgments section.[3]Current address: Cleveland Lou Ruvo Center for Brain Health, Cleveland Clinic, Cleveland, OH, USA.

*Corresponding author. Tel.: +49-341-9718000; Fax: +49-341-9718129.

E-mail address: osama.sabri@medizin.uni-leipzig.de

http://dx.doi.org/10.1016/j.jalz.2015.02.004

Abstract

Background: Evaluation of brain β-amyloid by positron emission tomography (PET) imaging can assist in the diagnosis of Alzheimer disease (AD) and other dementias.

Methods: Open-label, nonrandomized, multicenter, phase 3 study to validate the ^{18}F-labeled β-amyloid tracer florbetaben by comparing in vivo PET imaging with post-mortem histopathology.

Results: Brain images and tissue from 74 deceased subjects (of 216 trial participants) were analyzed. Forty-six of 47 neuritic β-amyloid-positive cases were read as PET positive, and 24 of 27 neuritic β-amyloid plaque-negative cases were read as PET negative (sensitivity 97.9% [95% confidence interval or CI 93.8–100%], specificity 88.9% [95% CI 77.0–100%]). In a subgroup, a regional tissue-scan matched analysis was performed. In areas known to strongly accumulate β-amyloid plaques, sensitivity and specificity were 82% to 90%, and 86% to 95%, respectively.

Conclusions: Florbetaben PET shows high sensitivity and specificity for the detection of histopathology-confirmed neuritic β-amyloid plaques and may thus be a valuable adjunct to clinical diagnosis, particularly for the exclusion of AD.

Trial registration: ClinicalTrials.gov NCT01020838.

Keywords: Amyloid; PET; Florbetaben; Histopathology

1. Introduction

Progress in research to improve diagnostic accuracy and treatment for Alzheimer disease (AD) depends on the characterization of underlying pathophysiologic mechanisms [1]. With estimates of more than a decade between the onset of β-amyloid deposition and cognitive decline in affected individuals, the opportunity exists to introduce effective disease-modifying regimens [2]. β-Amyloid imaging may aid this process by facilitating early diagnosis.

The International Working Group for New Research Criteria for the Diagnosis of AD recommends consideration of a dual clinicobiological process for diagnosis, involving the evidence of specific cognitive impairment together with biomarkers [3]. The recommendation was recently updated to categorize AD biomarkers according to whether they are involved in pathology or progression [4]. As the amyloid cascade is considered key to the pathogenesis of AD, β-amyloid is one such biomarker; existing techniques involve the imaging of β-amyloid plaques in the brain or detection of decreased β-amyloid levels in cerebrospinal fluid [5]. The successful use of such biomarkers has the potential to improve screening and diagnosis of AD. Amyloid imaging in particular is already being used as part of the eligibility criteria in large, multicenter clinical therapeutic trials.

Several ^{18}F-labeled β-amyloid ligands have been developed for positron emission tomography (PET) [6–9]. Phase 1 and 2 trials have been performed to study the pharmacokinetics, safety, and diagnostic efficacy of florbetaben [10–13]. Validating the accuracy of antemortem assessment of brain β-amyloid load requires correspondence between PET and histology-determined presence of β-amyloid deposits. Such validation has not been achieved to date because of technical challenges in ensuring the assessment of identical regions by PET readers and pathologists (for further details, see Supplemental Material). A pivotal histopathology phase 3 study is reported here in which the in vivo binding of florbetaben to β-amyloid was assessed by comparing whole-brain visual reads and quantitative analysis with the final neuropathological diagnoses of β-amyloid in the brain. In a subgroup, the visual assessment of slices with tissue-matched regions of interest (ROIs) on the PET scans was compared with the exact tissue-matched post-mortem brain tissue.

2. Methods

2.1. Study population

An international open-label, nonrandomized, multicenter phase 3 study (ClinicalTrials.gov: NCT01020838) was conducted in accordance with the Declaration of Helsinki. Approvals by regulatory authorities and ethics committees were obtained. Participants were recruited at 15 centers (including dementia clinics with brain bank experience, hospices, private practices, and dementia self-help groups) in Australia, Europe, Asia, and North America, and examined between February 2010 and July 2013. Patients with AD, dementia with Lewy bodies (DLB), or other dementias, and nondemented individuals, were included. Key exclusion criteria included severe cerebral large-vessel disease, brain tumors, and severe cardiovascular instability requiring intensive care surveillance or therapeutic intervention.

Participants (or their legal representatives) provided written informed consent to undergo brain magnetic resonance imaging (MRI), a PET scan with florbetaben, and to donate their brain for post-mortem examination. Participants received compensation for expenses incurred (e.g., travel), but no financial reward.

A cohort of young, cognitively normal healthy volunteers (age, 22–38 years), considered highly likely to be β-amyloid negative, was also recruited and studied by PET and MRI. Volunteers provided written informed consent before study procedures were carried out.

2.2. Brain image data acquisition

PET images were acquired from participants 90 to 110 minutes after intravenous injection of 300 MBq ± 20% florbetaben [14] according to a standardized acquisition and image-processing protocol established during a technical visit to each center. Three-dimensional volumetric T1-weighted brain MRI data (e.g., magnetization prepared rapid gradient echo or spoiled gradient recalled sequences) were also collected.

2.3. Post-mortem brain histopathology

Brain samples from participants who died during the study were used to determine the histopathology standard of truth.

For whole-brain analysis, amyloid histopathology was assessed according to the Consortium for Establishing a Registry for Alzheimer Disease (CERAD) scores [15]. Tissue was regarded as positive when sufficient neuritic plaques, detected by Bielschowsky silver staining, were present to meet criteria for AD (CERAD score of "frequent" or "moderate"). Histopathology was regarded as negative when the CERAD score was "absent" or "sparse." Diffuse plaques do not contribute to the CERAD score. The onsite pathologist conducted the autopsy (within 36 hours of death) and performed the CERAD scoring. In the first 31 brains examined, six brain regions were additionally dissected (middle frontal gyrus, occipital cortex, hippocampus/parahippocampal gyrus, anterior cingulate cortex, posterior cingulate cortex/precuneus, and cerebellar cortex). These regions were considered accessible for exact removal and suitable for coregistration and direct correlation of β-amyloid load as detected by in vivo PET imaging and post-mortem histopathology. Brain removal, cutting, block removal, photography, and embedding were performed according to a predefined standardized procedure (see Supplementary Material) to allow for alignment with the MRI and PET image data. Samples were processed for modified Bielschowsky silver staining [16] and immunohistochemistry (IHC) for a beta with the monoclonal 6E10 antibody (Zytomed Systems, Berlin, Germany) (see Supplementary Material) in a core laboratory. The same tissue-section was then identified in MRI and PET images. A section of up to 3.0 × 2.5 cm was used for each area for the histopathology assessment by a neuropathology consensus panel (three neuropathology experts) to semi-quantitatively determine the density of neuritic and diffuse plaques separately as absent, sparse, moderate, or frequent according to Mirra et al. [15].

For tissue-matched ROI analyses, an ROI was considered positive if there were moderate neuritic/cored or diffuse plaques, according to Bielschowsky silver staining or IHC. Diffuse plaques were identified based on the morphological appearance on either Bielschowsky silver staining or IHC and scored in the same way as neuritic plaques (see Supplementary Material).

2.4. PET image processing

Full description of MRI and PET image processing is provided in the Supplementary Material. Briefly, T1-weighted volumetric MRI for each participant was aligned with the photodocumented gross brain obtained at autopsy along the sagittal plane for coregistration. As the macroscopic pathology slices were cut at 1-cm intervals, the MRI was also "sliced" at 1-cm intervals. The accuracy of MRI slicing was compared against the photodocumented coronal pathology slices and, after several iterations, made to align precisely. Next, an ROI was drawn on the coronal MRI slices corresponding to the exact tissue region removed post-mortem for histopathological analysis. This was achieved by comparing the MRI with the photodocumented coronal slices showing where the tissue block had been extracted. Finally, the PET image was spatially normalized to the realigned MRI, and 1-cm-thick coronal PET images corresponding to the resliced MRI were obtained.

2.5. PET image data assessment

The comparison of whole-brain pathology with whole-brain imaging was made using a visual assessment method proposed for routine clinical use, developed to be independent of the availability of MRI scans. In a subgroup of participants, comparisons were made between regional brain pathology and tissue-matched ROIs placed on the PET scans (for more information, see Supplementary Material).

PET images were assessed by three in-person trained, independent readers who were blinded to the clinical and histopathology results. Whole-brain visual assessment used methodology adapted from previously described techniques [10,12]. This involved a regional cortical tracer uptake scoring system (1 = no tracer uptake, 2 = moderate tracer uptake, 3 = pronounced tracer uptake) in four brain areas, with the resulting scores condensed into a binary interpretation (score 1 = negative; score 2 or 3 = positive). In both whole-brain and tissue-matched ROI analyses, visual assessments were compared with histopathology results, and a majority-read approach was used to calculate diagnostic efficacy.

For the whole-brain quantitative analysis, composite cortical standardized uptake value ratios (SUVRs) were determined as previously described [12], and receiver operating characteristic (ROC) curve analysis was used to ascertain the optimal threshold for the sensitivity/specificity calculation. The SUVR that provided the highest sum of sensitivity and specificity as cutoff was determined.

2.6. Statistical analyses

Two-sided 95% confidence intervals (CIs) were calculated [17]. Sensitivity and specificity (see Supplementary Material) were evaluated using normal approximation with 95% CIs. Normal approximation/exact binomial distribution

with 95% CIs was used to evaluate the sensitivity and specificity of the whole-brain blinded read.

Inter- and intrareader agreements were estimated through kappa coefficients [18]. Differences between demographic parameters and SUVRs were tested using the independent two-sample *t*-test for continuous variables, or Fisher exact test for dichotomous variables. Correlations were calculated using Spearman correlation coefficients with 95% CIs. Analyses of variance (ANOVAs) together with the Tukey multiple comparison test were used to investigate the association between the composite SUVRs and the CERAD scores. Unless stated, all data are given as mean value ± standard deviation.

3. Results

3.1. Study population

Of 253 individuals screened, 218 (86%) were enrolled (Fig. 1), including 139 with a clinical diagnosis of AD, 5 with a clinical diagnosis of DLB, 31 with other dementias, 32 without dementia (primarily with oncological disorders), and 11 young, cognitively normal volunteers.

In total, 216 participants underwent florbetaben injection and PET imaging, including 205 end-of-life individuals (52% male; mean age, 76.9 ± 11 [range, 48–98] years) and 11 healthy volunteers. As of July 2013, 74 participants had died (mean age 80.4 ± 10.4 years; Supplementary Table 1) and undergone autopsy and post-mortem histopathology. The cohort included 57 patients with a clinical diagnosis of AD, 3 with DLB, 6 with other dementias, and 8 without dementia. The mean time from scan to death was 329 ± 272 days (Supplementary Table 1); 46 (62%) participants died within 1 year of the PET image being obtained, 20 (27%) within 2 years, and 8 (11%) after this time point. All 74 brains were used in the whole-brain analysis, and data from the first 31 participants who died formed the tissue-matched ROI-analysis subgroup. In addition, florbetaben PET data were analyzed from 10 young cognitively normal volunteers (the remaining volunteer was excluded because of a major protocol deviation).

3.2. Whole-brain analysis: Histopathology

The presence of neuritic β-amyloid plaques was confirmed in 47 of the 74 participants using histopathology, including only 44 of the 57 patients with a clinical diagnosis of AD, 1 of the 3 patients with DLB, 1 of the 6 individuals with "other" dementias, and 1 of the 8 individuals without dementia. Of the 13 patients with a clinical diagnosis of AD but no neuritic plaques, 12 had other neurodegenerative pathologies and 1 had no pathologically relevant changes. Overall, neuritic plaques were absent (i.e., "absent" or "sparse" neuritic plaque CERAD score) in 27 participants, including four with no neurodegenerative pathologies, and 23 with neurodegenerative pathologies other than AD (e.g., Parkinson's disease, Pick's disease and other forms of frontotemporal lobar degeneration, multisystem glial, and neuronal tauopathy).

3.3. Whole-brain analysis: Florbetaben PET

Scans were read as positive in 46 of the 47 cases with positive Bielschowsky silver staining (i.e., with moderate or frequent neuritic plaques on histopathology), and as negative in 24 of the 27 cases with sparse or absent neuritic plaques on histopathology. This resulted in a sensitivity of 97.9% (95% CI 93.8–100%) and a specificity of 88.9% (95% CI 77.0–100%) for florbetaben PET in detecting/excluding neuritic plaques ($\kappa = 0.90$ [95% CI 0.81–0.98]) (Table 1). The negative and positive predictive values for florbetaben PET were 96.0% (95% CI 88.3–100%) and 93.9% (95% CI 87.2–100%), respectively. A paradigmatic case with the brain regions to be assessed in the whole-brain analysis is shown in Supplementary Fig. 1. All four patients without neurodegenerative pathologies, and 20 of the 23 patients with non-AD neurodegenerative pathologies, were read as florbetaben PET negative.

The whole-brain quantitative florbetaben PET assessment included 73 scans; one was excluded because the MRI scan was of insufficient quality for gray versus white matter segmentation. Composite gray matter SUVRs were significantly higher in patients with β-amyloid plaques versus those without (1.71 ± 0.27 vs 1.24 ± 0.18; Fig. 2). ANOVA correlation analysis between CERAD scores and composite SUVRs found a highly significant ($P < .00001$) positive association. Tukey multiple comparison test showed significant differences in composite SUVRs between CERAD groups as follows: composite $SUVRs_{CERAD\ C}$ > composite $SUVRs_{CERAD\ 0}$ ($P < .00001$), composite $SUVRs_{CERAD\ C}$ > composite $SUVRs_{CERAD\ A}$ ($P = .0004$), composite $SUVRs_{CERAD\ B}$ > composite $SUVRs_{CERAD\ 0}$ ($P = .033$), and composite $SUVRs_{CERAD\ C}$ > composite $SUVRs_{CERAD\ B}$ ($P = .035$). ROC curve analysis of composite gray matter SUVRs resulted in a cutoff that allowed the whole-brain analysis group to be best separated into florbetaben-positive or florbetaben-negative brains. This was achieved with an SUVR of 1.478, resulting in a sensitivity of 89.4% (95% CI, 80.6–98.2%) and a specificity of 92.3% (95% CI, 82.1–100%) to detect β-amyloid plaques via florbetaben PET data quantification (Fig. 2).

3.4. Tissue-matched ROI analysis

Six ROIs matching the size and location of the six tissue blocks assessed by pathologists were placed on each of the scans from the first 31 patients who died. Similar ROIs were placed on scans from the 10 healthy volunteers (considered to be amyloid negative) (Fig. 1). In total, 244 tissue-matched ROIs were assessed, of which 106 were positive for plaques on histopathology.

A high level of interreader agreement was achieved for all brain ROIs ($\kappa = 0.66$) (Supplementary Table 2). Eighty-two of 106 ROIs were read as true PET positive, and 130 of 138 ROIs as true PET negative (Table 2; Fig. 3). In areas known to show β-amyloid plaques more frequently in AD (i.e., frontal cortex, anterior cingulate, posterior cingulate/precuneus

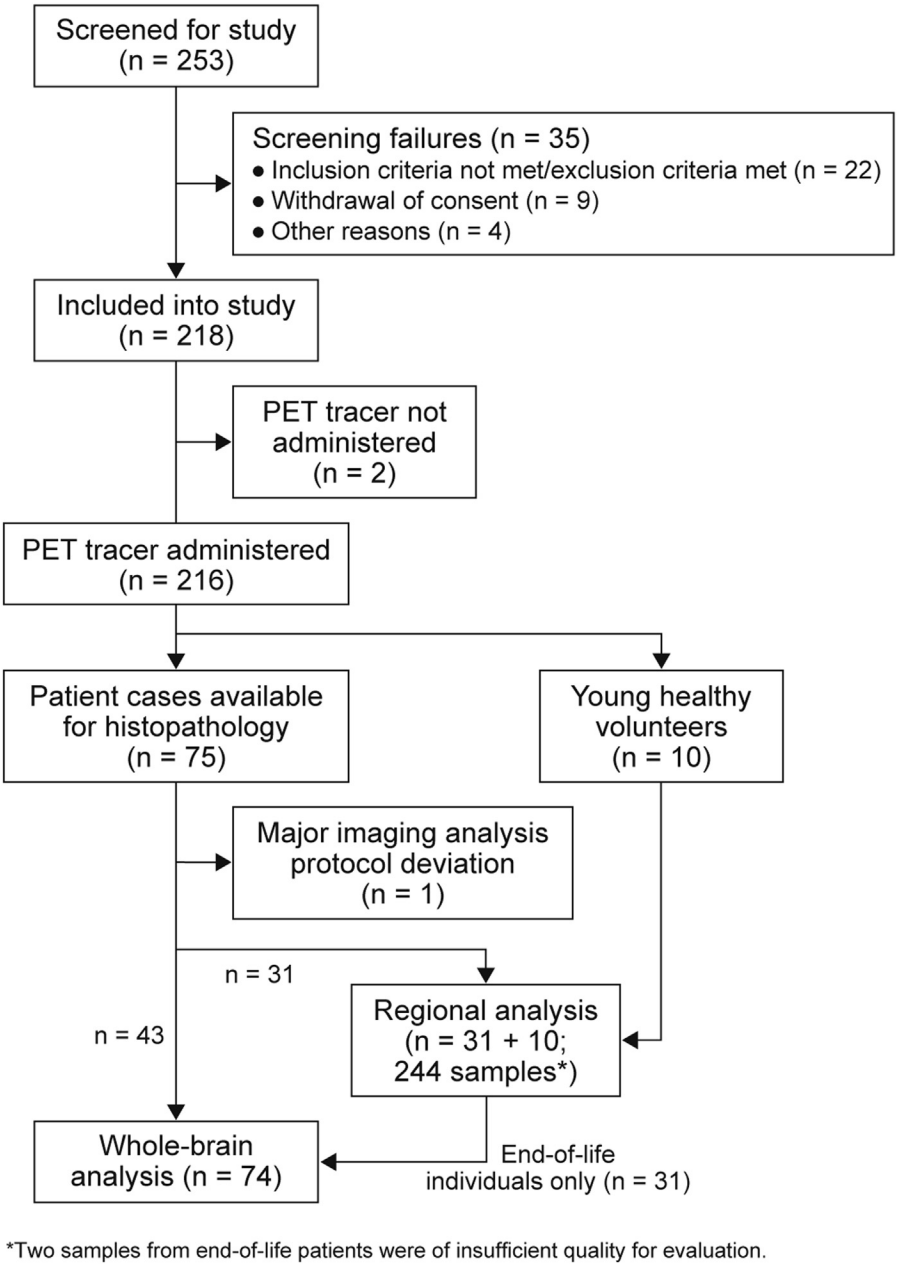

Fig. 1. Study flowchart of different trial stages. Two participants were enrolled but were not administered the positron emission tomography (PET) tracer as a result of death or adverse event after study inclusion. Ten healthy volunteers who were imaged with florbetaben in this trial were included by considering them as amyloid negative by definition. Tissue-matched region of interest (ROI) analysis was performed on a brain region-level basis considering central histopathology assessment by Bielschowsky silver staining and β-amyloid immunohistochemistry (IHC) as standard of truth with the first 31 available post-mortem cases. Whole-brain analysis was performed and compared against onsite histopathology assessment with the Consortium for Establishing a Registry for Alzheimer's Disease (CERAD) system as standard of truth in all 74 available post-mortem cases.

area), tissue-matched ROI sensitivity was 82–90%, and specificity was 86–95%. Sensitivity was lower (57%) but specificity higher (100%) for the hippocampus, resulting in an overall sensitivity of 77.4% (95% CI 65.3–89.4%) and a specificity of 94.2% (95% CI 88.6–99.8%) for all ROIs. In the tissue-matched ROI quantitative florbetaben PET assessment, significantly higher SUVRs were found for regions confirmed to have the histopathological evidence of β-amyloid compared with regions that were scored negative for β-amyloid, with the exception of the hippocampus/parahippocampal gyrus, consistent with the visual assessment (Table 2; Supplementary Fig. 2).

Regional florbetaben SUVRs correlated significantly with the consensus panel histopathology scores for neuritic and diffuse plaques in the middle frontal gyrus ($\rho = 0.62$ [95% CI 0.49–0.72]), occipital cortex ($\rho = 0.48$ [95% CI

Table 1
Visual assessment of florbetaben PET images by three blinded readers in the whole-brain analysis group (n = 74)

	Estimate	95% Lower CI	95% Upper CI
Sensitivity (%)			
Majority read	97.9	93.8	100.0
Reader 1	97.9	93.8	100.0
Reader 2	100.0	92.5	100.0
Reader 3	97.9	93.8	100.0
Specificity (%)			
Majority read	88.9	77.0	100.0
Reader 1	88.9	77.0	100.0
Reader 2	85.2	71.8	98.6
Reader 3	85.2	71.8	98.6

Abbreviations: PET, positron emission tomography; CERAD, Consortium for Establishing a Registry for Alzheimer's Disease; SUVRs, standardized uptake value ratios; CI, confidence interval.

NOTE. Onsite histopathology assessment by the CERAD criteria served as standard of truth.

0.33–0.61]), anterior cingulate cortex (ρ = 0.70 [95% CI 0.60–0.78]), and the posterior cingulate cortex/precuneus (ρ = 0.62 [95% CI 0.50–0.72]), but not in hippocampus/parahippocampal gyrus (ρ = 0.18 [95% CI 0.01–0.35]). The respective box plots are provided in Supplementary Fig. 3.

To determine the relationship between histopathologically determined plaque type and florbetaben uptake, neocortical gray matter ROIs with β-amyloid histopathology were considered: 21 with predominantly diffuse plaques, and 60 with both diffuse and neuritic plaques. In every instance, regions with neuritic plaques also had diffuse plaque deposition. No significant florbetaben SUVR differences were found between the two different plaque types, whereas both groups had significantly higher SUVRs compared with the plaque-negative ROIs (Fig. 2).

4. Discussion

Results from this study of florbetaben PET imaging to detect β-amyloid deposits in the brains of individuals with dementia demonstrate that the method used for the visual assessment was reliable and suitable for use in clinical practice. Indeed, florbetaben has been approved in the EU and USA in conjunction with a clinical evaluation, for PET imaging of β-amyloid neuritic plaque density in the brains of adult patients who are being evaluated for AD and other causes of cognitive impairment.

In the whole-brain analysis of 74 brains, the high sensitivity and specificity associated with the visual analysis (97.9% and 88.9%, respectively) were consistent with the sensitivity and specificity obtained using quantitative assessment of the PET images (89.4% and 92.3%, respectively). The sensitivity of the whole-brain analysis was, however, substantially higher than that of the tissue-matched ROI analysis. This is due in part to the lack of sensitivity in the hippocampus/parahippocampal gyrus. This region contains gray and white matter within a relatively small volume and is often atrophic, making it prone to partial volume effects. These characteristics made it difficult for the blinded imaging readers to properly assess this specific region. SUVR analysis for this region corroborated this difficulty in assessment. Importantly, florbetaben PET imaging had a high negative predictive value (96.0%), indicating that a PET scan evaluated as negative is a reliable indicator of the absence of sufficient plaque pathology in the brain to support a diagnosis of AD. In addition, the high positive predictive value confirms that florbetaben PET provides a reliable detection of plaques. It is important to note that the presence of β-amyloid plaques alone is not sufficient to diagnose AD, although cognitive impairment in the presence of β-amyloid plaques is strongly suggestive of AD. Consistent with previous studies, only 44 of 57 (77%) patients with a clinical diagnosis of AD in the present study were actually found to have brain β-amyloid [21].

The tissue-matched ROI validation of this study is the first direct, region-by-region anatomical comparison of an ^{18}F-labeled β-amyloid-targeted PET tracer uptake with post-mortem histopathologically determined β-amyloid load in matched tissue sections and imaging ROIs. In previous studies, in vivo versus post-mortem β-amyloid signal association was established solely using whole-brain PET assessment [22,23], which precluded detailed direct anatomic association between tracer uptake and β-amyloid plaques. Furthermore, PET data in previous studies were analyzed without corresponding the assessment of individual brain structural information provided by MRI. Our technique for region matching in vivo PET data with post-mortem histopathology data assured that identical brain regions were evaluated by both PET and histopathology readers, and that the gray matter was precisely separated within the ROIs from the white matter, where β-amyloid tracers are assumed to bind nonspecifically [24]. Hence, this study method provides an exact tissue-matched comparison of in vivo ROIs with post-mortem sections for validating the accuracy of florbetaben binding to β-amyloid.

Another advantage of this direct regional assessment of PET and histopathology was to allow the analysis of the ability of florbetaben to bind to diffuse and neuritic plaques. Although there is growing evidence that all β-amyloid deposits add to the course of AD [25], and the National Institute on Aging - Alzheimer's Association NIA-AA guidelines added nonneuritic β-amyloid deposition in form of modified Thal stages to the neuropathological assessment of AD [26], the binding of β-amyloid imaging agents to diffuse plaques is controversial and not well studied [27,28]. Here, we provide the largest

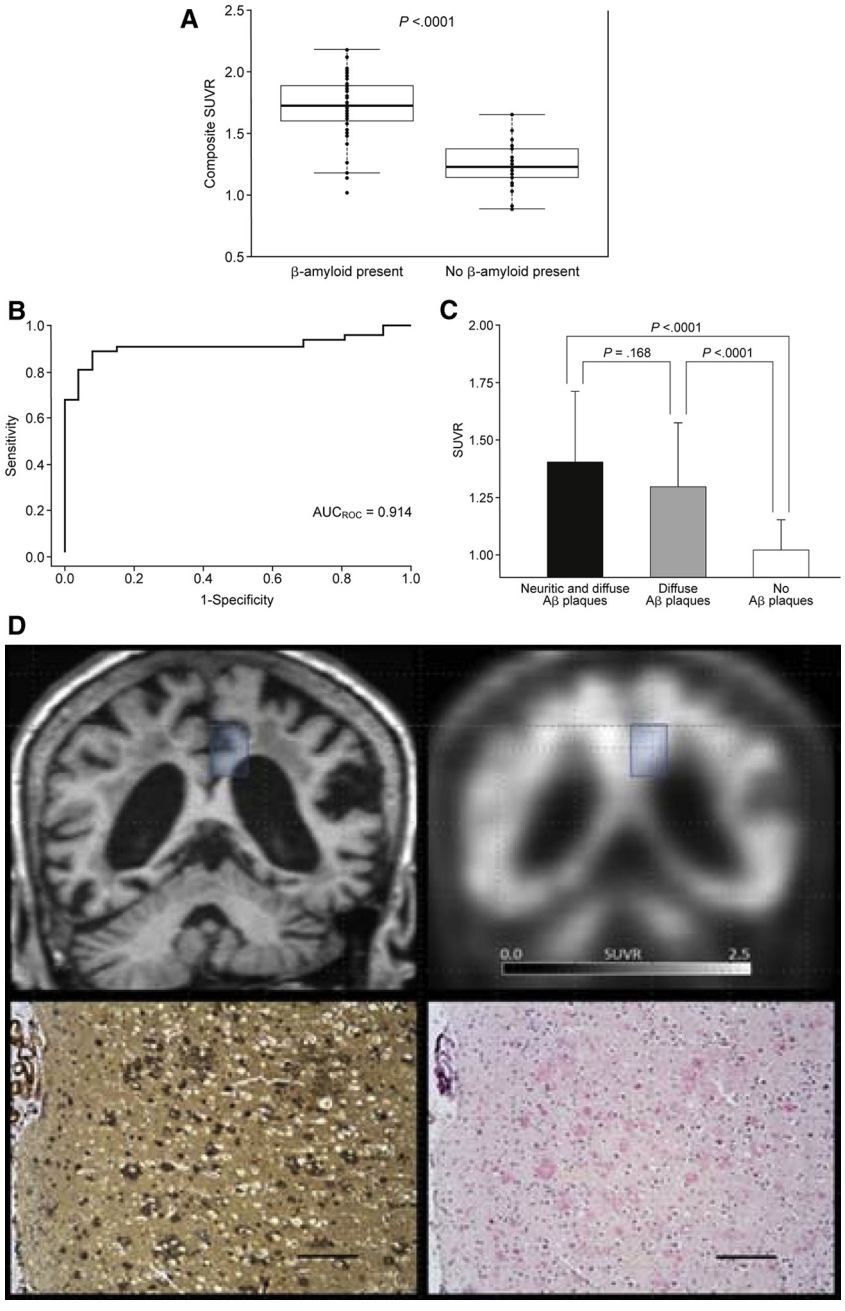

Fig. 2. Florbetaben uptake quantification in relation to brain plaque load and plaque types. (A) Boxplots of the composite standardized gray matter uptake value ratios (SUVRs) of florbetaben positron emission tomography (PET) imaging in whole-brain analysis group subjects with and without β-amyloid plaques. Mean SUVRs were compared against presence/absence of neuritic plaques as determined by onsite post-mortem histopathology according to Consortium for Establishing a Registry for Alzheimer's Disease (CERAD) criteria. The boxes show median values and first (Q1) and third (Q3) quartiles. The whiskers represent Q1 ± 1.5 of the interquartile ranges. (B) Receiver operating characteristic (ROC) curve for the composite gray matter SUVRs of florbetaben PET imaging in discriminating between whole-brain analysis group subjects with and without β-amyloid plaques. The area under the ROC curve was 0.914. According to this ROC statistics, the optimal separation SUVR threshold was determined as 1.48. Application of this cutoff SUVR resulted in a sensitivity and specificity of 89.4% and 92.3% of florbetaben PET in detecting β-amyloid plaques. (C) The influence of the β-amyloid plaque type as detected by centralized post-mortem histopathology using Bielschowsky silver staining and β-amyloid immunohistochemistry (IHC) in the tissue-matched gray matter region of interest (ROI) analysis group on the in vivo florbetaben uptake. Sixty ROIs exhibiting both diffuse and neuritic β-amyloid plaques were compared with 21 gray matter ROIs exhibiting predominantly diffuse β-amyloid plaques and 41 gray matter ROIs without β-amyloid plaques. Aβ, β-amyloid. (D) Florbetaben PET-positive case with predominantly diffuse plaque pathology. Coronal T1 magnetization prepared rapid gradient echo magnetic resonance (MR) slice (upper left) at the level of the posterior cingulate cortex/precuneus region of interest in which gray matter was segmented for gray matter PET analysis (blue box), corresponding coronal florbetaben PET slice (upper right) with posterior cingulate cortex/precuneus volume of interest (blue box) which was rated by the blinded readers as positive for cortical β-amyloid, corresponding post-mortem histopathology image of Bielschowsky silver staining (lower left) and IHC using monoclonal antibody 6E10 (lower right) predominantly exhibiting diffuse gray matter plaques. Black scale bars in histopathology images represent 200 μm.

Table 2
Region-level visual and quantitative assessment of post-mortem tissue-matched florbetaben PET images (tissue-matched ROI analysis of 244 brain regions)

		Tissue-matched ROI visual assessment (majority read)		Tissue-matched ROI quantitative assessment (SUVR)		
ROI (tissue matched)	Potential β-amyloid load	β-Amyloid in histopathology [TP/(TP + FN) (sensitivity [95% CI])]	No β-amyloid in histopathology [TN/(TN + FP) (specificity [95% CI])]	β-Amyloid in histopathology [mean ± SD (sensitivity [95% CI])*]	No β-amyloid in histopathology (mean ± SD (specificity [95% CI])[†]]	SUVR difference (95% CI)
Middle frontal gyrus	Intense [19]	18/21 (85.7% [70.7–100%])	19/20 (95.0% [85.4–100%])	1.30 ± 0.30** (90% [77.2–100%])	0.95 ± 0.12 (80% [62.5–97.5%])	0.35 (0.20–0.51)
Occipital cortex	Low [19]	16/18 (88.9% [74.4–100%])	19/22 (86.4% [72.0–100%])	1.34 ± 0.27** (89% [74.5–100%])	1.10 ± 0.10 (67% [47.3–86.4%])	0.23 (0.09–0.38)
Hippocampus/ parahippocampal gyrus	Low; significant atrophy [19,20]	12/21 (57.1% [36.0–78.3%])	20/20 (100% [83.1–100%])	0.99 ± 0.21 (71% [51.6–90.4%])	0.92 ± 0.17 (60% [38.5–81.4%])	0.07 (−0.08–0.22)
Anterior cingulate cortex	Intense [19]	18/20 (90.0% [77.0–100%])	18/21 (85.7% [70.7–100%])	1.36 ± 0.26*** (80% [62.4–97.5%])	0.96 ± 0.15 (100% [83.9–100%])	0.39 (0.24–0.54)
Posterior cingulate cortex/precuneus	Intense [19]	18/22 (81.8% [65.7–98.0%])	17/18 (94.4% [83.9–100%])	1.49 ± 0.35** (82% [66.0–98.0%])	1.06 ± 0.09 (100% [81.5–100%])	0.43 (0.26–0.59)
Cerebellar cortex	Reference [19]	0/4 (0.0% [0.0–60.2%])	37/37 (100% [90.5–100%])	[‡]	[‡]	
All		82/106 (77.4% [65.3–89.4%])	130/138 (94.2% [88.6–99.8%])			

Abbreviations: PET, positron emission tomography; ROI, region of interest; FN, false negative; FP, false positive; CERAD, Consortium for Establishing a Registry for Alzheimer's Disease; SUVR, standardized gray matter uptake value ratio using the cerebellar cortex as reference region; TN, true negative; TP, true positive; CI, confidence interval.

NOTE. Centralized histopathology assessment using Bielschowsky silver staining and β-amyloid IHC served as the standard of truth. Column 2 describes knowledge from literature on the usual amount of β-amyloid load in case of AD in the ROIs deliberately selected in this study to obtain a wide spectrum with different degrees of expected β-amyloid pathology. Group differences were tested for significance using the *t*-test for independent samples.

*$P < .05$; **$P < .01$; ***$P < .001$ vs "no β-amyloid histopathology."

[†]Derived from receiver operating characteristic curve analyses.

[‡]Reference region for SUVR calculation.

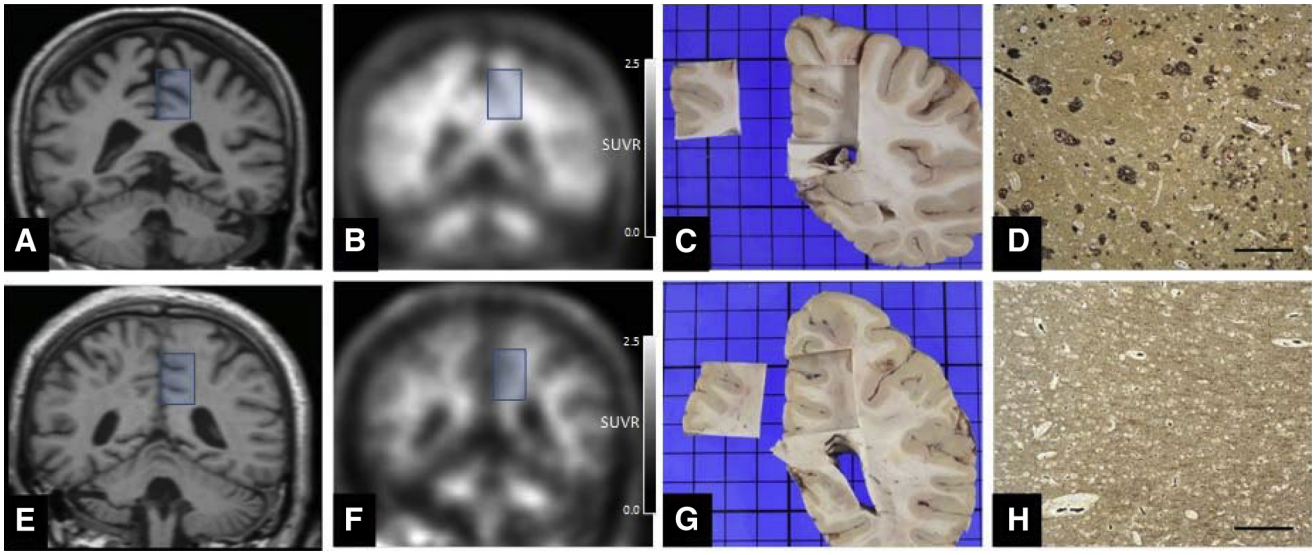

Fig. 3. Two paradigmatic tissue-matched region of interest (ROI) analysis examples. The upper row shows results from a β-amyloid-positive patient (Case 48) and the lower row shows findings from a β-amyloid-negative patient (Case 45). Coronal T1 magnetization prepared rapid gradient echo magnetic resonance (MR) slices at the level of the posterior cingulate cortex/precuneus ROI (A, E), corresponding coronal florbetaben positron emission tomography (PET) slices (B, F), corresponding post-mortem coronal brain slice photodocumentation (C, G), and corresponding histopathology images (black scale bars representing 200 μm) of Bielschowsky silver staining (D, H). Based on the photodocumented size and position of the posterior cingulate cortex/precuneus brain blocks, which were removed post-mortem, respective ROIs were defined on the individual in vivo MRI and coregistered florbetaben PET imaging data (blue boxes). Note that PET/MRI versus brain slice coregistration was optimized toward the ROI, as it was not possible to perfectly fit all brain parts in the respective slices due to post-mortem brain shrinkage and deformation. Within the ROIs, the gray matter was segmented for tracer uptake analysis. In concordance with the results of the Bielschowsky silver staining that revealed plaque positivity (D) and negativity (H), cortical florbetaben uptake was evident (B), and absent (F).

set of brain sections with an appropriate methodology to confirm that florbetaben binds to both neuritic and diffuse plaques in vivo.

One limitation of the study, which is also applicable to other comparisons of in vivo β-amyloid PET imaging with post-mortem histopathology [22,23], is that clinical features of end-of-life individuals had significant end-stage medical illnesses that could bias the PET data. For example, some patients had pronounced brain atrophy, which made visual assessment of the PET scans challenging, negatively biasing the association between the PET and histopathology signals. Furthermore, the possibility cannot be excluded that the pharmacodynamics and pharmacokinetics of β-amyloid-targeted PET tracers are different in end-of-life patients compared with earlier stage patients in whom PET has greater clinical relevance and in whom future clinical application is desired. If β-amyloid PET imaging is to be used routinely in the clinical assessment of such patients, then there is a need for large-scale controlled diagnostic trials in patients in the early stages of dementia [12]. Only such studies, together with pivotal in vivo PET versus post-mortem histopathology comparisons as carried out in the present study, will provide the full picture of the clinical efficacy of β-amyloid PET imaging as an adjunct to clinical assessment for early, ante-mortem diagnosis of AD and prodromal AD.

In conclusion, high sensitivity and specificity, and high predictive values for florbetaben PET, were confirmed by histopathology in clinically relevant whole-brain visual analyses, allowing the reliable detection and exclusion of amyloid pathology. Moreover, this study involved the rigorous validation of florbetaben PET in an exact tissue-matched ROI analysis. These data, together with the results from earlier studies [10–12,14,29–31], support the value of florbetaben PET as a diagnostic marker, particularly as a valuable adjunct for the exclusion of AD or differential diagnosis of dementia.

Acknowledgments

Medical writing support was provided by Dan Booth (Bioscript Medical, London, UK) and funded by Piramal Imaging S.A. Additional statistical analysis was carried out by Santi Bullich (Piramal Imaging GmbH).

The trial was funded by Bayer Pharma AG, Berlin (Germany), and Piramal Imaging S.A., Matran (Switzerland). Bayer Pharma AG was involved in the design of the study; Bayer Pharma AG and Piramal Imaging SA were involved in the conduct of the study; collection, management, analysis, and interpretation of the data; and in the preparation, review, and approval of the manuscript.

Professor Osama Sabri and Professor Marwan Sabbagh had full access to all the data in the study and take

responsibility for the integrity of the data and the accuracy of the data analysis.

Investigators of the florbetaben phase 3 study group

Australia: C. Rowe, P. Yates, K. Young, C. Masters, C. McLean [Melbourne].

France: F. Pasquier, A. Rollin, V. Deramecourt, G. Petyt, F. Semah, J. F. Legrand, T. Prangere, C. A. Maurage [Lille], F. Blanc, B. Cretin, N. Philippi, J. Namer, S. Kremmer, C. Hammer, J. Detour, B. Lannes [Strasbourg].

Germany: E. Steinhagen-Thiessen, O. Peters, B. Janen, M. Rudolphs, B. Heinig, A. Huppertz, D. Behrendt, S. Dresel [Berlin], M. Haupt, H.-H. Friedemann, A. Hufnagel [Duesseldorf], A. Bauer, D. Kremer, T. Kroll, D. Elmenhorst, A. Matusch [Julich], O. Sabri, H. Barthel, H.-J. Gertz, B. Eggers, S. Hesse, S. Tiepolt, K.-T. Hoffmann [Leipzig].

Japan: H. Akatsu, J. Hashizume, A. Hori, R. Kurihara, Y. Saitou, M. Ishii, K. Senda [Aichi], B. Mihara, Y. Yoshida [Gunma], M. Sakamoto, Y. Ouchi [Shizuoka], S. Murayama, K. Ishii, M. Takao, A. Tokumaru, H. Hatsuta, K. Kanemaru, K. Eguchi, M. Sunakawa, M. Shiina, T. Komiya, Y. Nishina, Y. Hiroyoshi, T. Komiya, Y. Nishina [Tokyo].

USA: K. Womack, R. Diaz-Arrastia, M. Devous, D. Mathews, C. White [Dallas], N. Rasgon, S. Gambhir, T. Wroolie, M. Trockel, T. Robakis, E. Mittra, M. Vasanawala, R. Sobel [Palo Alto], E. Melhem, M. Bilello, J. Dubroff, C. Divgi, Z. Mourelatos, A. Barr [Philadelphia], J. Gutierrez, P. Fox, F. Sharkey, R. Moreno [San Antonio], M. Sabbagh, S. Charney, C. H. Adler, S. Jacobsen, F. Schummner, T. Beach [Sun City], B. A. Raj, A. Smith, H. Chheda, G. Clark, F. R. Murtagh, L. Hair [Tampa], J. Brunetti, S. Wagle, S. Stravinski, A. Vergara, M. A. Paris, C. D. Katsetos, R. Ownbey [Teaneck].

Central Pathology: W. J. Schulz-Schaeffer, A. Wrede [Goettingen, Germany].

Pathology Consensus Panel Readers: J. W. Ironside [Edinburgh, UK], B. Ghetti [Indianapolis, USA], J. B. Leverenz [Seattle, USA].

Molecular Neuroimaging, LLC.: J. Seibyl, G. Zubal, S. Mendick, K. Marek, and the entire MNI team [New Haven, USA].

Bayer Pharma AG: C. Reininger, A. Hoffmann, C. Pfefferer, B. Hesse, G. Holl, B. Putz, R. Braun, M. Kunz, K. Roth, M. Hildenbrand, J. Kuhlmann, and the global study team.

Piramal Imaging GmbH on behalf of Piramal Imaging S.A.: M. Berndt, S. Bullich, A. Catafau, L. Dinkelborg, M. Friebe, J. Hirschfeld, N. Koglin, A. Mueller, A. Stephens, S. Thomsen.

Supplementary data

Supplementary data related to this article can be found at http://dx.doi.org/10.1016/j.jalz.2015.02.004.

RESEARCH IN CONTEXT

1. Systematic review: Only one clinical trial with two publications [22,23] is reported in PubMed comparing an ^{18}F-labeled β-amyloid agent against autopsy-derived histopathology.
2. Interpretation: In our study, which is the second to be reported meeting the aforementioned criteria, florbetaben positron emission tomography (PET) was investigated in a global phase 3 trial. A high diagnostic efficacy was determined for the detection of neuritic plaques in 74 deceased subjects. In a subgroup, an exact tissue-scan matched analysis was performed in 244 samples. As such, it is the first trial to directly compare PET regions ante-mortem to identical tissue regions analyzed post-mortem. Florbetaben PET confirmed efficacy for the in vivo detection of β-amyloid deposits, both on a whole brain and on a regional brain level.
3. Future directions: Trials testing β-amyloid PET in the early dementia stage are needed and the influence of plaque morphology on the PET signal needs to be further explored.

References

[1] Vandenberghe R, Adamczuk K, Dupont P, Laere KV, Chetelat G. Amyloid PET in clinical practice: its place in the multidimensional space of Alzheimer's disease. Neuroimage Clin 2013;2:497–511.

[2] McGeer PL, McGeer EG. The amyloid cascade-inflammatory hypothesis of Alzheimer disease: implications for therapy. Acta Neuropathol 2013;126:479–97.

[3] Dubois B, Feldman HH, Jacova C, Cummings JL, Dekosky ST, Barberger-Gateau P, et al. Revising the definition of Alzheimer's disease: a new lexicon. Lancet Neurol 2010;9:1118–27.

[4] Dubois B, Feldman HH, Jacova C, Hampel H, Molinuevo JL, Blennow K, et al. Advancing research diagnostic criteria for Alzheimer's disease: the IWG-2 criteria. Lancet Neurol 2014;13:614–29.

[5] Jack CR Jr. Alzheimer disease: new concepts on its neurobiology and the clinical role imaging will play. Radiology 2012;263:344–61.

[6] Nelissen N, Van LK, Thurfjell L, Owenius R, Vandenbulcke M, Koole M, et al. Phase 1 study of the Pittsburgh compound B derivative 18F-flutemetamol in healthy volunteers and patients with probable Alzheimer disease. J Nucl Med 2009;50:1251–9.

[7] Cselényi Z, Jönhagen ME, Forsberg A, Halldin C, Julin P, Schou M, et al. Clinical validation of 18F-AZD4694, an amyloid-beta-specific PET radioligand. J Nucl Med 2012;53:415–24.

[8] Wong DF, Moghekar AR, Rigamonti D, Brašić JR, Rousset O, Willis W, et al. An in vivo evaluation of cerebral cortical amyloid with [18F]flutemetamol using positron emission tomography compared with parietal biopsy samples in living normal pressure hydrocephalus patients. Mol Imaging Biol 2013;15:230–7.

[9] Small GW, Kepe V, Ercoli LM, Siddarth P, Bookheimer SY, Miller KJ, et al. PET of brain amyloid and tau in mild cognitive impairment. N Engl J Med 2006;355:2652–63.
[10] Barthel H, Luthardt J, Becker G, Patt M, Hammerstein E, Hartwig K, et al. Individualized quantification of brain beta-amyloid burden: results of a proof of mechanism phase 0 florbetaben PET trial in patients with Alzheimer's disease and healthy controls. Eur J Nucl Med Mol Imaging 2011;38:1702–14.
[11] Villemagne VL, Ong K, Mulligan RS, Holl G, Pejoska S, Jones G, et al. Amyloid imaging with (18)F-florbetaben in Alzheimer disease and other dementias. J Nucl Med 2011;52:1210–7.
[12] Barthel H, Gertz HJ, Dresel S, Peters O, Bartenstein P, Buerger K, et al. Cerebral amyloid-beta PET with florbetaben (18F) in patients with Alzheimer's disease and healthy controls: a multicentre phase 2 diagnostic study. Lancet Neurol 2011;10:424–35.
[13] Rowe CC, Ackerman U, Browne W, Mulligan R, Pike KL, O'Keefe G, et al. Imaging of amyloid beta in Alzheimer's disease with 18F-BAY94-9172, a novel PET tracer: proof of mechanism. Lancet Neurol 2008;7:129–35.
[14] Becker GA, Ichise M, Barthel H, Luthardt J, Patt M, Seese A, et al. PET quantification of 18F-florbetaben binding to beta-amyloid deposits in human brains. J Nucl Med 2013;54:723–31.
[15] Mirra SS, Heyman A, McKeel D, Sumi SM, Crain BJ, Brownlee LM, et al. The Consortium to Establish a Registry for Alzheimer's Disease (CERAD). Part II. Standardization of the neuropathologic assessment of Alzheimer's disease. Neurology 1991;41:479–86.
[16] Yamamoto T, Hirano A. A comparative study of modified Bielschowsky, Bodian and thioflavin S stains on Alzheimer's neurofibrillary tangles. Neuropathol Appl Neurobiol 1986;12:3–9.
[17] Rao JN, Scott AJ. A simple method for the analysis of clustered binary data. Biometrics 1992;48:577–85.
[18] Fleiss JL. Statistical methods for rates and proportions. 2nd ed. Hoboken, NJ: John Wiley & Sons Ltd; 1981.
[19] Braak H, Braak E. Neuropathological staging of Alzheimer-related changes. Acta Neuropathol 1991;82:239–59.
[20] Scheltens P, Leys D, Barkhof F, Huglo D, Weinstein HC, Vermersch P, et al. Atrophy of medial temporal lobes on MRI in "probable" Alzheimer's disease and normal ageing: diagnostic value and neuropsychological correlates. J Neurol Neurosurg Psychiatry 1992;55:967–72.
[21] Beach TG, Monsell SE, Phillips LE, Kukull W. Accuracy of the clinical diagnosis of Alzheimer disease at National Institute on Aging Alzheimer Disease Centers, 2005–2010. J Neuropathol Exp Neurol 2012;71:266–73.
[22] Clark CM, Schneider JA, Bedell BJ, Beach TG, Bilker WB, Mintun MA, et al. Use of florbetapir-PET for imaging beta-amyloid pathology. JAMA 2011;305:275–83.
[23] Clark CM, Pontecorvo MJ, Beach TG, Bedell BJ, Coleman RE, Doraiswamy PM, et al. Cerebral PET with florbetapir compared with neuropathology at autopsy for detection of neuritic amyloid-beta plaques: a prospective cohort study. Lancet Neurol 2012;11:669–78.
[24] Stankoff B, Freeman L, Aigrot MS, Chardain A, Dollé F, Williams A, et al. Imaging central nervous system myelin by positron emission tomography in multiple sclerosis using [methyl-(1)(1)C]-2-(4'-methylaminophenyl)- 6-hydroxybenzothiazole. Ann Neurol 2011;69:673–80.
[25] Thal DR, Griffin WS, Braak H. Parenchymal and vascular Abeta-deposition and its effects on the degeneration of neurons and cognition in Alzheimer's disease. J Cell Mol Med 2008;12:1848–62.
[26] Hyman BT, Phelps CH, Beach TG, Bigio EH, Cairns NJ, Carrillo MC, et al. National Institute on Aging-Alzheimer's Association guidelines for the neuropathologic assessment of Alzheimer's disease. Alzheimers Dement 2012;8:1–13.
[27] Sabbagh MN, Fleisher A, Chen K, Rogers J, Berk C, Reiman E, et al. Positron emission tomography and neuropathologic estimates of fibrillar amyloid-beta in a patient with Down syndrome and Alzheimer disease. Arch Neurol 2011;68:1461–6.
[28] Ikonomovic MD, Klunk WE, Abrahamson EE, Mathis CA, Price JC, Tsopelas ND, et al. Post-mortem correlates of in vivo PiB-PET amyloid imaging in a typical case of Alzheimer's disease. Brain 2008;131(Pt 6):1630–45.
[29] Villemagne VL, Mulligan RS, Pejoska S, Ong K, Jones G, O'Keefe G, et al. Comparison of 11C-PiB and 18F-florbetaben for Abeta imaging in ageing and Alzheimer's disease. Eur J Nucl Med Mol Imaging 2012;39:983–9.
[30] Schipke CG, Peters O, Heuser I, Grimmer T, Sabbagh MN, Sabri O, et al. Impact of beta-amyloid-specific florbetaben PET imaging on confidence in early diagnosis of Alzheimer's disease. Dement Geriatr Cogn Disord 2012;33:416–22.
[31] Fodero-Tavoletti MT, Brockschnieder D, Villemagne VL, Martin L, Connor AR, Thiele A, et al. In vitro characterization of [18F]-florbetaben, an Abeta imaging radiotracer. Nucl Med Biol 2012;39:1042–8.